Detailed Investigation of Mode-Field Adapters Utilizing Multimode-Interference in Graded Index Fibers

Peter Hofmann, Arash Mafi, Clémence Jollivet, Tobias Tiess, N. Peyghambarian, and Axel Schülzgen

***Abstract*—We present a detailed study of mode-field adapters (MFA) based on multimode interference in graded index multimode fibers. We have fabricated and characterized MFAs from a selection of commercially available single-mode and graded index fibers. Compared to existing techniques, the presented MFAs can be fabricated very quickly and are not limited to certain fiber types. Insertion losses of < 0.5 dB over a spectral range of several hundred nanometers have been obtained, which is comparable or better than the industry standard.**

***Index Terms*—Graded index fiber, mode-field adapter, multimode-interference, self-imaging.**

I. Introduction

With an ever-increasing variety of commercially available single-mode fibers and rising popularity of single-mode fiber devices, a strong demand to efficiently couple light between single-mode fibers with dissimilar mode-field diameters (MFD) has developed. Traditionally, mode-field adapting has been achieved using biconical tapering [1] or mode-field expansion by thermal diffusion of the core [2], [3], or a combination of both [4]. Some of these techniques have matured into commercial products and although these techniques are providing adapters with low insertion losses on the order of 0.5 dB or better, the manufacturing process can be quite time consuming, the width of the spectral response is usually on the order of tens of nanometers, and the resulting products cost easily several hundreds to a thousand of dollars.

Here, we propose a method based on multimode interference in graded index multimode fiber (GIMF) that can overcome these limitations. In multimode fibers, different modes propagate with different group velocities, which results in an interference pattern along the fiber. For a finite number of excited modes, the interference pattern is periodic along the fiber. This effect is known as self-imaging. In fibers, it was first demonstrated by Allison and Gillies [5]. Since then, a variety of its properties and applications [6]–[15] have been studied successfully. Self-imaging occurs when the initial phase relation between the modes is recovered. However, since the number of excited modes in step index multimode fibers can be rather large and their propagation constants are not evenly spaced, it becomes almost impossible to have the exact same phase relationship repeated within a reasonable length of fiber. Hence, the reproduced field shows aberrations which can be quantified by a self-imaging quality factor [7], [8]. In striking contrast, GIMFs that are commonly used in telecommunications to reduce group velocity dispersion for increased bandwidth exhibit much more evenly spaced propagation constants and fewer guided modes and, consequently, their self-imaging length can be drastically shorter when compared to step index fibers.

We recently demonstrated [16] that under certain conditions multimode interference in GIMFs can be utilized to significantly reduce the coupling loss between mode-field mismatched single-mode fibers forming a simple low-cost MFA suitable for large-scale production. Little attention has been paid to GIMFs outside the telecommunications field. They have been used in combination with lensed fiber tips for fiber coupling schemes [17] or in biomedical applications [18], [19].

In this paper, a detailed numerical and experimental study of GIMF-based MFAs is presented. In the first part, we perform a numerical analysis on mode excitation and mode propagation in three different GIMFs for different excitation conditions. From there, we then find the self-imaging lengths for the GIMFs using optimization capabilities of the commercial Fimmwave software suite. In the second part, we experimentally investigate MFAs with different combinations of single-mode fibers and GIMFs and show that the predictions from the previously derived mathematical formalism [16] hold for a large range of fiber parameters. We demonstrate that under certain conditions, the coupling loss can be reduced to almost zero, whereas in other cases the insertion of a GIMF can actually increase the loss. To characterize the MFAs, the transmission behavior has been investigated in the spectral domain. In the last part, experimental results for wavelength tuning are shown and an MFA of short length with minimized wavelength dependence is presented.

Manuscript received January 23, 2012; revised March 26, 2012 and April 16, 2012; accepted April 16, 2012. Date of publication April 25, 2012; date of current version May 23, 2012. This work was supported by the National Science Foundation under Grant 0725479. The work of A. Mafi was supported by the UWM Research Growth Initiative Grant.

P. Hofmann is with the CREOL College of Optics and Photonics, University of Central Florida, Orlando, FL 32816 USA, and also with the College of Optical Sciences, University of Arizona, Tucson, AZ 85721 USA (e-mail: phofmann@optics.arizona.edu).

A. Mafi is with the Department of Electrical Engineering and Computer Science, University of Wisconsin-Milwaukee, Milwaukee, WI 53211 USA (e-mail: mafi@uwm.edu).

C. Jollivet, T. Tiess, and A. Schülzgen are with the CREOL College of Optics and Photonics, University of Central Florida, Orlando, FL 32816 USA (e-mail: jollivet@creol.ucf.edu; tobias.tiess@knights.ucf.edu; axel@creol.ucf.edu).

N. Peyghambarian is with the College of Optical Sciences, University of Arizona, Tucson, AZ 85721 USA (e-mail: nasser@optics.arizona.edu).

Color versions of one or more of the figures in this paper are available online at http://ieeexplore.ieee.org.

Digital Object Identifier 10.1109/JLT.2012.2196406

II. Mode Analysis and Excitation in GIMF

When light is coupled from a single-mode fiber to a multimode fiber, the number of excited modes and their fractional power depends on the parameters of both single and multimode fiber as well as on the wavelength of the coupled light. We first examine the modal composition inside different GIMFs for the case that 1550 nm light is launched from a Corning smf28e single-mode fiber. We assume perfect angular and lateral alignment between any two coupled fibers. Three different commercially available GIMFs have been considered in this study. They all exhibit a nearly parabolic index distribution in the core, which is described by

$$n^2(\rho) = n_0^2\left[1 - 2\Delta\left(\frac{\rho}{R}\right)^{\alpha}\right]. \quad (1)$$

Here, n_0 is the refractive index at the center of the core, Δ is the fractional refractive index difference, and ρ and R are the radial coordinate and the radius of the core, respectively. The value of α is nearly 2.0, though its exact value depends on the optical and geometrical characteristics of each individual GIMF. Table I shows the GIMF parameters at 1550 nm wavelength that have been used in our simulations. For all three fibers, the cladding material was assumed to be undoped fused silica glass, for which the Sellmeier coefficients are well known [20]. With these parameters, we numerically calculated the mode fractional power of the LP modes exited in the respective GIMF. As expected, only modes with zero angular momentum ($\mathrm{LP}_{0,\mathrm{n}}$) are excited since all devices studied here exhibit cylindrical symmetry and the light is always launched concentrically. We find that there are six radially symmetric modes excited in the GIF62.5, compared to five in the GIF50 and nine in the GIF100. The transverse intensity distributions of these excited $\mathrm{LP}_{0,\mathrm{n}}$ modes are shown in the left part of Fig. 1. For comparison, the modes of a SI50 step index multimode fiber with 50 μm core diameter and a numerical aperture of 0.22 are also provided. It can be seen that for increasing mode indices, the fields of the GIMF modes extend further toward the cladding compared to the modes of the step index fiber, for which the mode-field covers roughly the same area for all modes. In the upper part of Fig. 1, the calculated propagation constants of the excited $\mathrm{LP}_{0,\mathrm{n}}$ modes are plotted for the three GIMFs and the SI50 steps index fiber. While the propagation constants of the GIMFs are evenly spaced, those of the step index fibers are not. Next, we analyze the excitation amplitudes of the various modes excited inside the multimode fibers using the commercial mode solver Fimmwave. As shown in our previous study [16], the excitation amplitude distribution between different modes as well as the total power fraction (sum) coupled from the single mode to the multimode fiber depends on both single- and multimode fiber parameters. First, we again consider the case that 1550 nm light is launched from a Corning smf28e single mode into various multimode fibers. The calculated fractional powers of the excited $\mathrm{LP}_{0,\mathrm{n}}$ modes are shown in Fig. 2(a). Note that the data in Fig. 2 are plotted on a logarithmic scale. For all GIMFs, most of the power is coupled to the fundamental mode and the mode fractional power is rapidly decreasing for higher order modes. This is different from what is observed in the SI50 step index fiber. Here, several modes are excited more homogeneously, which is due to the large diameter of the fundamental mode of the SI50 when compared to the in-coupling Gaussian mode-field. In Fig. 2(b), we show similar data for the case that 1550 nm light originating from different single-mode fibers is coupled into the same GIMF GIF50. It is shown that both the amplitude distribution as well as the total fractional power depend strongly on the single-mode fiber parameters such as the mode-field radius w and the numerical aperture. In particular, the total coupling loss depends nonlinearly on the mismatch between w and the mode-field radius of the fundamental mode in the graded index fiber ρ_c. As shown in Fig. 2(b), the highest coupling efficiency is reached when the MFD of the in-coupling single-mode fiber is close to the fundamental MFD of the GIF50 fiber. For example, only 0.2 dB of coupling loss is expected, when coupling LMA12 to GIF50. On the other hand, losses of 2 dB are calculated for coupling the strongly mismatched single-mode fiber UHNA7 to GIF50. The data also indicate that even for a relatively small number of excited modes (e.g., 5 for GIF50) light can be coupled almost lossless to the GIMFs from single-mode fibers with a wide range of MFDs. The excitation amplitudes are also slightly wavelength dependent. The effect of a wavelength change can be seen in Fig. 2(c), where we studied the coupling between smf28e and the GIMF GIF62.5. The observed changes in modal amplitude distribution are due to the wavelength dependence of ρ_c and w of the considered fibers as well as different cutoff wavelengths for the individual modes of the GIMFs.

III. Propagation of Multimode Fields

After discussing the excitation of multiple modes, we will analyze the electromagnetic field propagating inside the GIMFs. At each location along the fiber, a characteristic pattern will be formed due to the interference of the excited modes. In Fig. 3(a)–(c), these patterns are shown for GIF50 after 1550 nm light has been launched from three different single-mode fibers, namely (a) UHNA7, (b) LMA12, and (c) LMA25. The key parameters for these fibers are provided in Table II.

If the in-coupling mode-field is very small relative to the graded index fibers fundamental mode [see Fig. 3(a)], several higher order modes are excited rather homogeneously and form a periodic interference pattern. However, the limited number of available modes limits the coupling efficiency to the GIMF. If the mode-field is very similar to the fundamental mode size of the GIMF, as it is the case in Fig. 3(b), the fundamental mode of the GIMF is dominantly excited and only one other mode carries significant power. Only if the in-coupling beam diameter is not too much different (can be larger or smaller) from the GIMF fundamental mode diameter, the GIMF's higher order modes are excited efficiently and a strong interference pattern is generated that is also carrying almost all of the launched power [see Fig. 3(c)].

Next, as illustrated in Fig. 3(d), the transmission through a chain of smf28e-GIMF-smf28e has been calculated as a function of GIMF length for all three GIMFs under consideration.

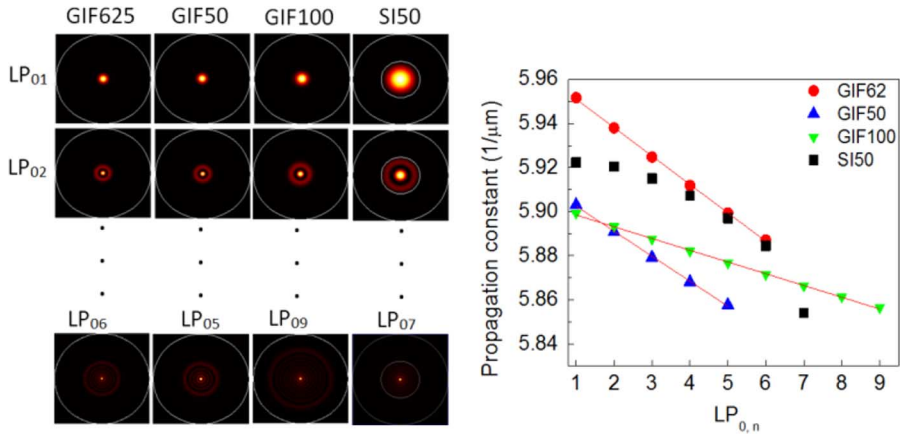

Fig. 1. (Left) Circularly symmetric $LP_{0,n}$ modes in GIMFs and SI50 step index fiber with comparable core diameter. The mode-field area for the GIMF increases with increasing mode index, whereas it is approximately constant for the step index fiber. (Right) Propagation constants of the circularly symmetric modes in GIMF and a comparable step index fiber. Note the even spacing of the propagation constants of the GIMF $LP_{0,n}$ modes.

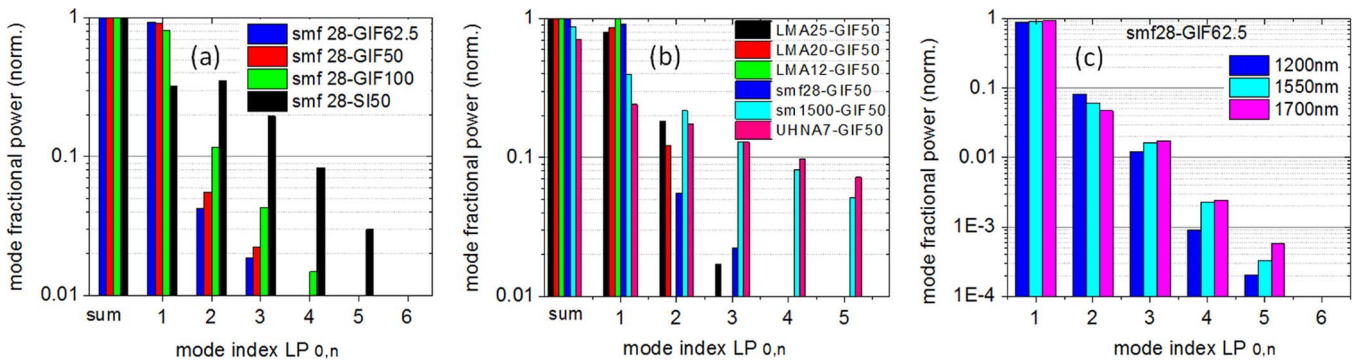

Fig. 2. (a) Calculated excitation amplitudes of azimuthally symmetric modes in various graded index multimode fibers and for comparison in a SI50 step index multimode fiber. The light was launched from a smf28e single-mode fiber at 1550 nm. (b) Total coupled power and mode fractional power in GIF50 fiber for launching light from various single-mode fibers with decreasing MFDs. High coupling efficiencies can be obtained even if the MFD of the single-mode fiber is quite different from the LP_{01} MFD of the GIMF. (c) Wavelength dependence of the modal composition in GIF62.5; since the MFD are a function of wavelength, the excitation amplitudes vary also with wavelength.

TABLE I
KEY PARAMETERS OF GRADED AND STEP INDEX MULTIMODE FIBERS USED IN THIS STUDY ($\lambda = 1550$ NM)

Fiber	Core diameter [μm]	Cladding diameter [μm]	Numerical aperture	MFD $LP_{0,1}$ [μm]
GIF625	62.5	125	0.275	14.9 ±1
GIF50	50	125	0.2	16.9 ±1
GIF100	100	140	0.18	22.7 ±1
SI50	50	125	0.22	38.0 ±2

TABLE II
KEY PARAMETERS OF STEP INDEX SINGLE-MODE FIBERS USED IN THIS STUDY ($\lambda = 1550$ NM)

	Core diameter [μm]	Cladding diameter [μm]	Numerical aperture	MFD $LP_{0,1}$ [μm]
LMA25	25	400	0.06	24 ±2
LMA20	20	125	0.07	21 ±1
LMA15	15	200	0.07	18 ±1
LMA12	12	125	0.08	14.8 ±1
FUD3583	9.6	125	0.10	14 ±1
smf28e	8.2	125	0.12	10.6 ±1
HI780	4.2	125	0.14	9 ±1
sm1500	4.2	125	0.27	5 ±0.5
UHNA7	3.2	125	0.38	4 ±0.5

As shown in Fig. 3(e), multimode interference leads to a modulation of the transmission versus GIMF length where transmission maxima occur at the characteristic length for self-imaging which is different for the different GIMFs due to their variations in modal index dispersion as shown on the right side of Fig. 1. For all three GIMFs, the first self-imaging peak occurs after propagating approximately 1 mm or less inside the multimode fiber. This is in strong contrast to the step index multimode fiber SI50, where the first self-imaging peak is observed after approximately 10 mm, as shown in Fig. 3(f). In addition, the unequal spacing of the modal indexes in SI50 leads to much stronger variations in the multimode interference patterns resulting in huge differences in transmission for different multimode fiber lengths. Experimentally, it is much easier to analyze multimode interference effects in the frequency domain. Since the self-imaging length is wavelength dependent [8], the interference pattern as well as the transmission of a fiber chain such as in Fig. 3(d) will be a function of the wavelength. That means, by gradually changing the wavelength, we can scan through the interference pattern in the longitudinal direction. To demonstrate this effect, a 45.8 cm piece of GIF50 was spliced to smf28e and

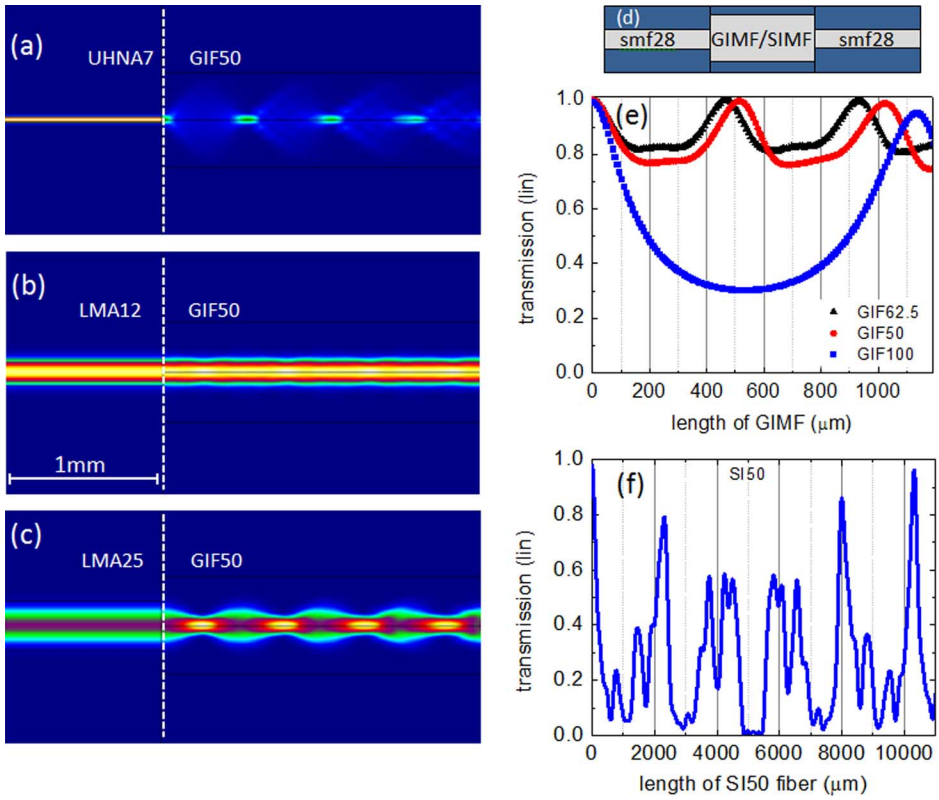

Fig. 3. (a)–(c) Calculated interference pattern inside GIF50 fiber for increasing MFDs of the in-coupling fiber. (d) and (e) Self-imaging length in GIMF is on the order of 1000 μm and increases with number of strongly excited modes. (f) Compare to SI50 fiber, where the power is more homogeneously distributed among available modes, the self-imaging length is increased by an order of magnitude.

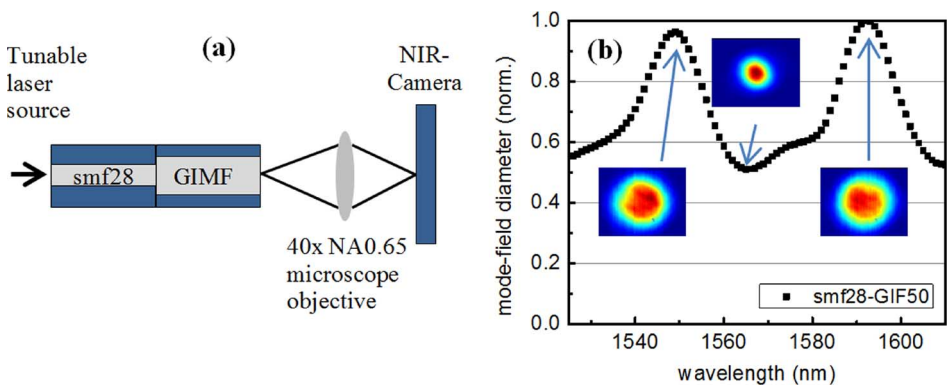

Fig. 4. (a) Experimental setup for mode-field imaging. (b) Measured MFDs as a function of launched wavelength with three mode-field image examples.

light from a tunable laser source was launched from the smf28e fiber into the GIMF. Using a 40x microscope objective and an NIR camera, the mode-field at the exit facet of the multimode fiber was imaged onto the camera. A schematic of the experimental setup is provided in Fig. 4(a). In our experiment, the wavelength was scanned in increments of 1 nm from 1525 to 1610 nm. In order to compensate for chromatic aberration of the imaging system, the image plane was adjusted slightly each time the wavelength was changed. In Fig. 4(b), the measured MFDs are plotted as a function of wavelength, together with three recorded images illustrating the breathing of the interference pattern between fields with small and large diameters.

IV. Direct Coupling of Single-Mode Fibers

Suppose now light needs to be coupled between two single-mode fibers with different MFDs. Neglecting angular tilt and lateral offset, the power coupled from the core mode of the input fiber to the core mode of the output fiber is well approximated by

$$T = \frac{P_1}{P_2} = \frac{4w^2 w'^2}{\left(w^2 + w'^2\right)^2} \tag{2}$$

where w and w' are the $1/e^2$ mode-field radii of the two single-mode fibers, respectively [21]. This formula predicts that coupling losses between single-mode fibers can be rather high. For example, when coupling from an LMA20, which has an MFD of approximately 21 μm to standard smf28e with an MFD of 10 μm the expected coupling loss is 40% or 2.2 dB at a wavelength of 1550 nm. This coupling loss is also wavelength dependent due to the wavelength dependence of the MFDs of the single-mode fibers.

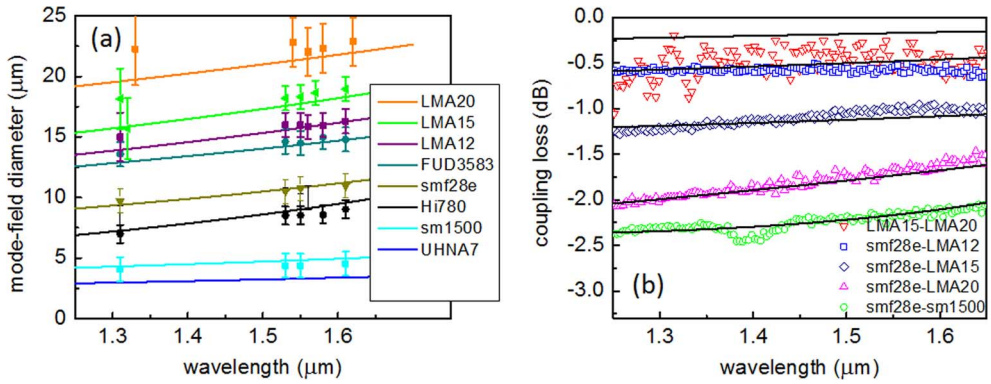

Fig. 5. (a) Measured and calculated MFDs of single-mode fibers used in the experiments. (b) Measured and calculated direct coupling loss for some single-mode fiber combinations studied in this paper.

An accurate knowledge of the direct coupling loss between the respective single-mode fibers is the key starting element for studying the performance of MFAs. From (2), we see that the accuracy of the result relies on the precise knowledge of w and w'. Since manufacturers rarely provide the MFD for more than two wavelengths and the uncertainty associated with these values can be fairly large in some cases, we found it appropriate to measure the MFD at different wavelengths between 976 and 1610 nm for the single-mode fibers under consideration. There is a variety of methods available to measure MFDs of fibers [22]. Here, we used a technique known as near-field method, where the tip of the fiber is reimaged onto an NIR camera, allowing measurement of the MFD by image processing. The near-field method has its limitations for fibers with MFDs that approach the diffraction limit of the imaging system [23]—usually a microscope objective. Commercially available step index single-mode fibers range typically from about 3 μm for ultra-high numerical aperture fibers to 30 μm for large mode area (LMA) fibers with low numerical apertures of about 0.06. In this study, we imaged the core of the respective fiber onto an Indigo Alpha NIR camera with a 320×256 pixel array and a 30×30 μm pixel-size. A $40\times$ microscope objective with $\mathrm{NA} = 0.65$ was used and a Gaussian fit was applied to the so obtained image. The measurement results are shown in Fig. 5(a). The line plots are obtained by fitting Marcuse equation [21] to the measured mode-fields, where cutoff wavelength and core radius where used as the fitting parameters within the provided manufacturers' tolerances.

It can be seen that the measurement method is limited to fibers that are single mode at the measurement wavelength. Below the cutoff wavelength, due to the onset of higher order modes, the measured values arise from a superposition of all excited modes rather than the fundamental mode only and it is hence no longer possible to find a good agreement with Marcuse equation. For example, LMA20 is not truly single mode anymore in this wavelength range ($\lambda_c \sim 2$ μm for LMA20). For fibers with small MFDs, the imaging method is limited by the point spread function of the objective, which is typically on the order of 2–3 μm. Here, we found good agreements between predicted values and measured values for fibers with MFDs from 5 to 20 μm. The so obtained wavelength dependent MFDs have been used to calculate direct coupling losses using (2). The direct coupling losses were also measured using a white-light source and an optical spectrum analyzer and compared to the calculated direct coupling losses. Results for different fiber combinations are plotted in Fig. 5(b). The measured results are in good agreement with the calculations, the only exception being the case when coupling the two LMA fibers: LMA15 and LMA20. This can be explained by the onset of multimode excitation in both fibers due to the fact that both fibers are tested close to or even below their respective cutoff wavelength. In addition to that the LMA15 fiber has a cladding diameter of 200 μm compared to 125 μm for all other fibers, making splicing a challenging task. Note also the slight wavelength dependence of the direct coupling loss due to a wavelength dependency of w and w'.

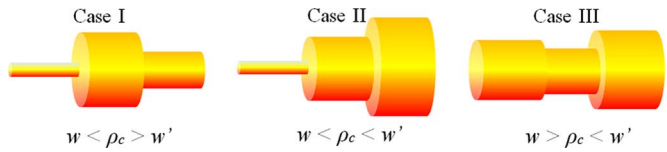

Fig. 6. Three distinct cases of combining different single-mode fibers through a GIMF segment can be distinguished considering the sizes of the respective mode radii. Only case II actually improves the coupling efficiency between the two single-mode fibers and almost lossless coupling is achieved when $\eta\eta' = 1$.

V. Mode-Field Adapters With GIMF

Next, we will demonstrate how to utilize a segment of GIMF between two different single-mode fibers to strongly reduce the coupling losses. If a graded index fiber of length L with a characteristic radius of its fundamental mode ρ_c is inserted between two single-mode fibers, it has been shown [16] that the transmission can be approximated by

$$T(L,\lambda) = \left[\frac{(\eta+\eta')^2}{4\eta\eta'} \cos^2\left(\frac{\pi L}{Z}\right) + \frac{(1+\eta\eta')^2}{4\eta\eta'} \sin^2\left(\frac{\pi L}{Z}\right) \right]^{-1} \quad (3)$$

where

$$\eta = \frac{\rho_c^2}{w^2}, \quad \eta' = \frac{\rho_c^2}{w'^2} \quad (4)$$

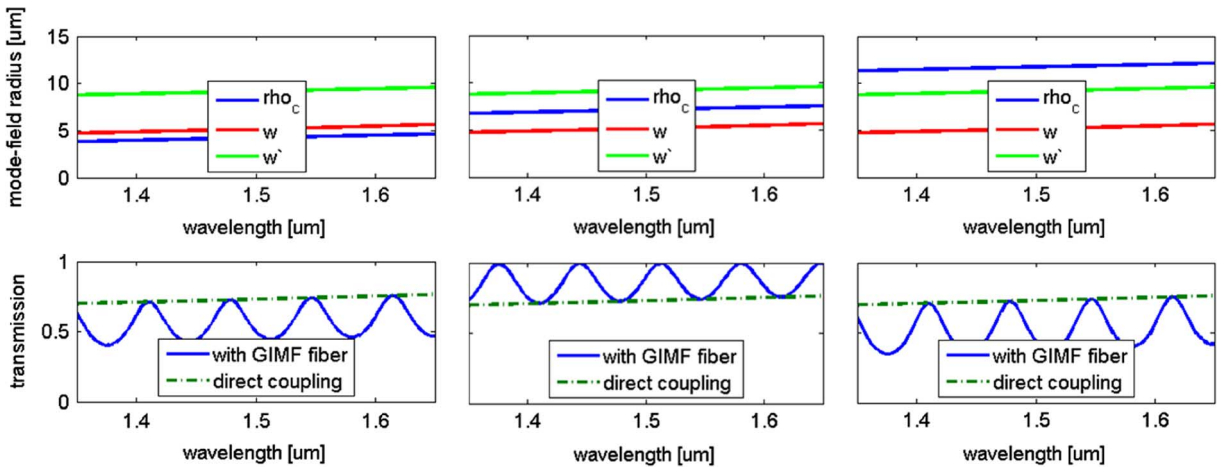

Fig. 7. (Media 1) Single-frame excerpts corresponding to each case from Fig. 6, respectively. The animation shows a gradually increasing ρ_c (upper plots) and its effect on the transmission spectrum of the MFA (lower graphs). The mode-field radii w and w' are calculated for single-mode fibers smf28 and LMA20 respectively using Marcuse equation [21].

are the ratios between the mode-field radii of the respective single-mode fiber w and w' and the characteristic radius of the fundamental GIMF mode ρ_c. This transmission is a periodic function of the GIMF segment length and the wavelength. The spectral periodicity of the interference pattern is given by

$$Z(\lambda) = \frac{\pi R}{\sqrt{2\Delta(\lambda)}} \tag{5}$$

where R is the core radius of the GIMF and Δ is the fractional index difference between the center of the GIMF core and its cladding [see (1)]. In general, Δ is wavelength dependent where the exact functional form of the wavelength dependence is not readily available from fiber manufacturers or literature. It can, therefore, only be estimated by comparing experimental results with measured data. Here, we found that over the wavelength range between 1260 and 1650 nm, it is mostly sufficient to use a linear approximation to fit the measured transmission spectra (a quadratic fit was used for the GIF62.5—fiber)

$$\Delta(\lambda) = \Delta + \delta(\lambda - \lambda_c). \tag{6}$$

We now want to show how the MFA's transmission function is related to η. This can be thoroughly visualized by setting $w < w'$ and plotting the transmission of the MFA (3) as a function of wavelength while gradually increasing ρ_c.

By looking at the movie in Fig. 7, the three cases can be distinguished, as shown in Fig. 6. For case I, the MFDs of the single-mode fibers are both smaller than ρ_c resulting in $w < w' < \rho_c$ so $\eta < 1$ and $\eta' < 1$. Case II occurs when $w < \rho_c < w'$, and for case III the mode-field radii of the single-mode fibers are both larger than ρ_c giving $\rho_c < w < w'$. It can be shown [16] that for cases I and III the peaks of the transmission function are given by

$$\tau(z_{\text{even}}) = \tau(0) = \frac{4\eta\eta'}{(\eta+\eta')^2}\left[1 - (\Psi\Psi')^P\right]^2 \tag{7}$$

where

$$\Psi = \frac{\eta - 1}{\eta + 1}, \quad \Psi' = \frac{\eta' - 1}{\eta' + 1}.$$

Analyzing this equation for a varying number P of guided zero angular momentum modes in the GIMF, we can see that the factor $(\psi\psi')^P$ approaches zero for increasing P and (7) approaches (2), Marcuse's formula for the direct coupling loss of dissimilar single-mode fibers [21]. In fact, the transmission for cases I and III can never exceed the transmission for direct coupling. In striking contrast, for case II, the transmission will always be equal or higher than the direct coupling transmission (the functions minima coincide with the direct coupling loss for the two single-mode fibers) and can reach unity when $\eta\eta' = 1$. Again from [16] for case II MFAs, the transmission maxima are given by

$$\tau(z_{\text{even}}) = \tau(0) = \frac{4\eta\eta'}{(\eta+\eta')^2}\left[1 - (\Psi\Psi')^P\right]^2. \tag{8}$$

We note that (7) and (8) are consistent with (3), considering the fact that the $(\psi\psi')^P = 0$ approximation is already adopted in (3). Therefore, only for fiber chains that represent case II, the multimode fiber actually improves the coupling loss, while for all other cases the loss increases.

In order to visualize now what happens inside a case II MFA, a FIMMPROP simulation of a GIF50 fiber with $L = nZ + Z/2$ inserted between smf28e and LMA20 fiber has been performed. The results can be seen in Fig. 8(a). The output fiber entrance facet is placed exactly where the periodic interference pattern matches the mode-field of the out-coupling fiber making low loss coupling possible. Fig. 8(b) shows the calculated transmission versus GIMF length at a fixed wavelength of 1550 nm. It can be seen that the coupling efficiency is indeed periodic with $L$with a periodicity of $Z = 0.5$ mm.

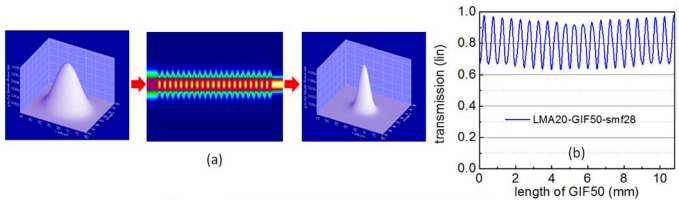

Fig. 8. (a) Calculated intensity distribution of an LMA20-GIF50-smf28e MFA. The graded index fiber carries the multimode interference pattern used to image the input mode-field onto the output fiber entrance facet. (b) Calculated transmission versus GIMF length.

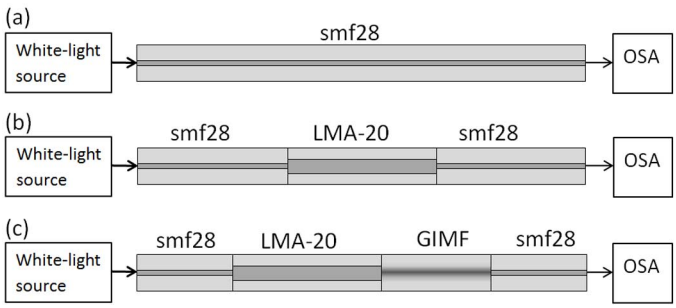

Fig. 9. Experimental setup used to characterize the MFAs. (a) First, a baseline is recorded. (b) Then, the second single-mode fiber is added via fusion splicing and two times the direct coupling loss is obtained. (c) As a third step, the GIMF is inserted and another transmission spectrum is recorded.

A. Mode-Field Adapter With Different Combinations of GIMF and SMF

In order to experimentally verify the GIMF MFA approach for a wider range of single-mode fibers, ten MFAs have been fabricated. The individual fiber sections have been fusion spliced to each other using a conventional Ericsson FSU 995 fusion splicer. The transmission through each device has then been measured over a wavelength range from 1260 to 1650 nm and compared to the direct coupling loss. A schematic of the performed sets of experiments is shown in Fig. 9.

The light from a single-mode fiber coupled super-continuum source is used to excite the fundamental core mode of the input single-mode fiber of the mode-field-adapter under test. Cladding modes were stripped out by the high-index polymer coating of the fiber. For double cladded fibers like the LMA20, potential cladding modes were stripped out by applying index matching fluid around the splice region. As discussed previously, at the splicing point to the GIMF several radially symmetric modes are excited inside the graded index fiber.

After propagating through the GIMF (multimode interference), the light couples back into the output single-mode fiber at the exit surface of the graded index fiber. The output fiber is then connected to an optical spectrum analyzer to record the transmission spectrum. To obtain accurate values for the transmission loss of the MFA, the measurement must be carefully calibrated to account for splice losses between all the fiber segments of the MFA. To do this, first a baseline measurement has been performed with the smf28e fiber going directly from the source into the OSA [see Fig. 9(a)]. Then, without removing any of the FC-APC connectors, the second single-mode fiber was

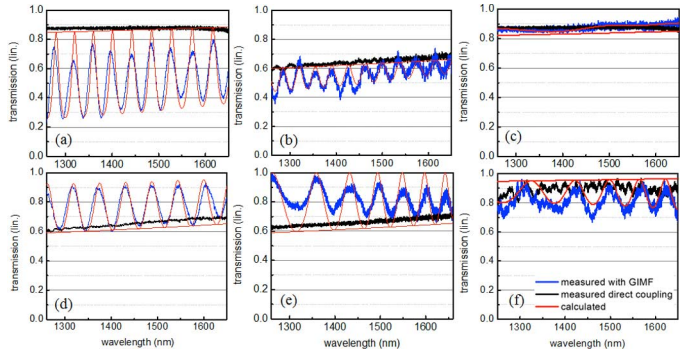

Fig. 10. Calculated and measured transmission spectra of graded index multimode fiber MFAs shown in Table III. ww'/ρ_c^2 is increasing from (a) to (f), resulting in adapters from each of the three cases of Fig. 9. Strongly improved transmission can be achieved for the couplers in (d) and (e) that fall into category II. In the other cases, the coupling losses increase in the presence of the multimode fiber. For the case of $ww'/\rho_c^2 = 1$, the MFA works best and the transmission approaches unity (e).

TABLE III
FIBER COMBINATIONS USED FOR MFA

	$\frac{ww'}{\rho_c^2}$	in-coupling SMF	GIMF	Length of GIMF (cm)	out-coupling SMF
(a)	0.30	smf28e	GIF100	12.8	LMA12
(b)	0.44	smf28e	GIF100	14.7	LMA20
(c)	0.71	smf28e	GIF62.5	22.2	LMA12
(d)	0.79	smf28e	GIF50	29.8	LMA20
(e)	1.02	smf28e	GIF62.5	81.1	LMA20
(f)	1.73	LMA15	GIF62.5	65.6	LMA20

fusion spliced in between the smf28e fiber and another transmission spectrum has been recorded [see Fig. 9(b)]. The difference between the baseline and this spectrum represents the direct coupling losses for two connections. Since both fibers are single mode, the direct coupling losses for both connections are identical and the loss per splice can be found by dividing the measured total loss by two. Now, the graded index fiber section was spliced between the two different single-mode fibers and a third transmission spectrum has been recorded [see Fig. 9(c)]. From these data, the known loss of the remaining direct coupling point has been subtracted to obtain the overall transmission of the MFA. Table III exemplifies six of the fiber combinations that have been fabricated. Measured and calculated transmission spectra for these MFAs are shown in Fig. 10. The calculated spectra were obtained by plotting (3) versus wavelength. In Fig. 10(a), the transmission through a LMA12-GIF100-smf28e MFA is shown.

This MFA falls in category I, where the MFDs of both single-mode fibers are smaller than the fundamental mode-field of the GIF fiber. As expected, only the transmission maxima (almost) reach the level of the transmission for direct coupling. Starting from (a) going to (f), the ratio ww'/ρ_c^2 is increasing, resulting in still type I MFA for (b) and (c), type II MFA for (d) and (e) and a type III MFA for (f). Discrepancies between theory and experiment may be attributed to mode conversion and/or imperfect excitation conditions both resulting in modified multimode interference patterns. An interesting observation is made

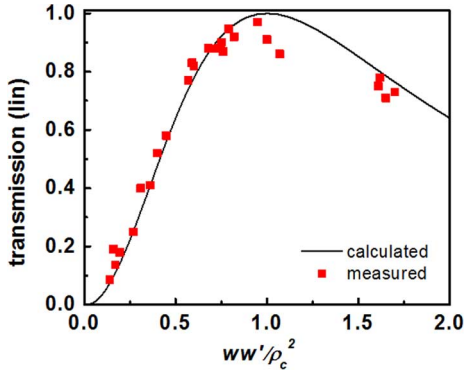

Fig. 11. Peak (valley) transmission through various MFAs as a function of ww'/ρ_c^2. The measured values are obtained from the maxima (minima) of the transmission spectra at different wavelengths.

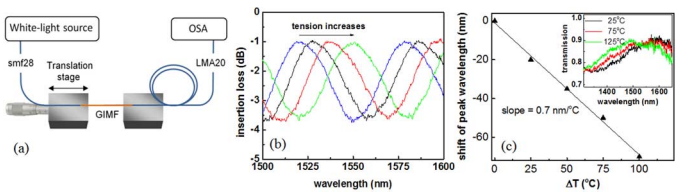

Fig. 12. (a) Experimental setup used for wavelength tuning of MFA. (b) Transmission spectrum through the smf28e-GIF50-LMA20 adapter for different levels of tension. The transmission spectrum can be tuned to peak at any wavelength. (c) Temperature dependence of MFA transmission peak. Inset: MFA transmission spectra at selected temperatures.

when the MFD of either one of the single-mode fibers matches the mode-field of the fundamental mode of the graded index fiber, as it is the case in (c). The modulation amplitude is now strongly reduced, indicating that the MFD of the graded index fiber GIF62.5 is close to the MFD of the LMA12 fiber. The light couples directly to the fundamental mode of the GIMF fiber without exciting higher order modes, or in the reversed light case, only the fraction of light that is in the fundamental mode couples to the LMA12 fiber. The coupling loss with graded index fiber is therefore very similar to the direct coupling loss. Fig. 10(c) also marks the transition between cases I and II. At this point, the spectrum "flips" about the axis for the direct coupling loss. Fig. 10(d) and (e) represents the case II where the transmission maxima are given by (8) and the addition of the GIMF segment results in an improved transmission when compared to the direct coupling case.

The measured transmission spectra of (d) and (e) clearly confirm this, and a maximum transmission of almost unity is reached when ww'/ρ_c^2 reaches one in (e). If the ratio is further increased, the spectrum flips again, the device becomes a type III MFA [see Fig. 10(f)] and the coupling loss increases again when compared to the direct coupling loss. The measured spectrum here suffers from noise. This is most likely caused by fiber deformation in the splice regions of the LMA15 fiber. Since this fiber has a cladding diameter of 200 μm and is spliced on both ends to fibers with 125 μm cladding diameter (smf28e and GIF62.5), the fiber geometry in the splice region will be altered during the fusion process. However, the measured transmission spectrum still clearly confirms the theoretical predictions. While the transmission spectra of Fig. 10 already suggest a good agreement between theory and experiment, we can convince ourselves even more by plotting the MFA peak/valley transmission as a function of ww'/ρ_c^2. These data are shown in Fig. 11. Red dots represent measured peak/valley transmission values. The solid line is calculated from (3) using the fundamental MFDs obtained experimentally in Section 1. Since the ratio ww'/ρ_c^2 is wavelength dependent (due to the wavelength dependence of the MFDs), several measurement points (2 to 3) were obtained from each MFA. The measured results show excellent agreement with the theoretical predictions.

B. Temperature and Strain Sensitivity of Mode-Field Adapters

As seen in Fig. 10, the improved transmission of the MFAs is wavelength and GIMF length dependent. To operate at a particular wavelength, the length of the GIMF segment has to be accurately controlled. Cleaving a 30 cm long section of fiber to a length accuracy of about 20 μm can be achieved but this is not trivial. Therefore, spectral fine tuning of the transmission peaks is highly desirable. This may be achieved by mechanically stretching the GIMF fiber section or by changing the temperature of the MFA or a combination of both. First mechanical tension was applied to the graded index fiber section. The experimental setup is provided in Fig. 12(a). A smf28e-GIF50-LMA20 MFA with an approximate length of 30 cm has been fixed on one end of the GIMF and mounted to a translation stage on the other end. Fig. 12(b) shows the transmission spectrum through this device for different levels of tension. It is possible to apply enough tension to the piece of GIF50 fiber in order to shift the transmission pattern by at least half a period, making accurate cleaving of the GIF less critical or perhaps more importantly, allowing to use the same MFA at different wavelengths. Second, the influence of temperature changes on the mode-field adaptors transmission spectrum has been examined. For this experiment, we fabricated an MFA using the same fibers as in Table III (d) with a length of 4.4 cm instead. We then placed the adapter on a heater plate and increased its temperature from 25 °C to 125 °C in steps of 25 °C. For each temperature, a transmission spectrum has been measured. We found that the interference pattern shifted towards shorter wavelengths with 0.7 nm/°C temperature increase (see Fig. 12(c) with inset).

C. Mode-Field Adapters With Increased Spectral Bandwidth

While the previously described MFAs may be used in certain environments, they exhibit a limited bandwidth and are relatively sensitive to bending and vibrations due to their length. It is possible to overcome both limitations by making the GIMF section very short. By analyzing (3), it can be seen that reducing L will also lead to a slower modulation of the $\cos^2$ and $\sin^2$ terms, therefore reducing the wavelength dependence and increasing the width of the pass band. For a demonstration of such a short MFA, we used again the combination of smf28e—GIF50-LMA20 since it showed the best performance in the previous experiments. FIMMWAVE simulations suggest that the first transmission maximum for this particular combination of fibers and a wavelength of 1550 nm occurs for a GIF-length of 258 μm. In order to achieve such an accurate control over the fiber length, a cleaver has been mounted under a conventional microscope and the smf28e

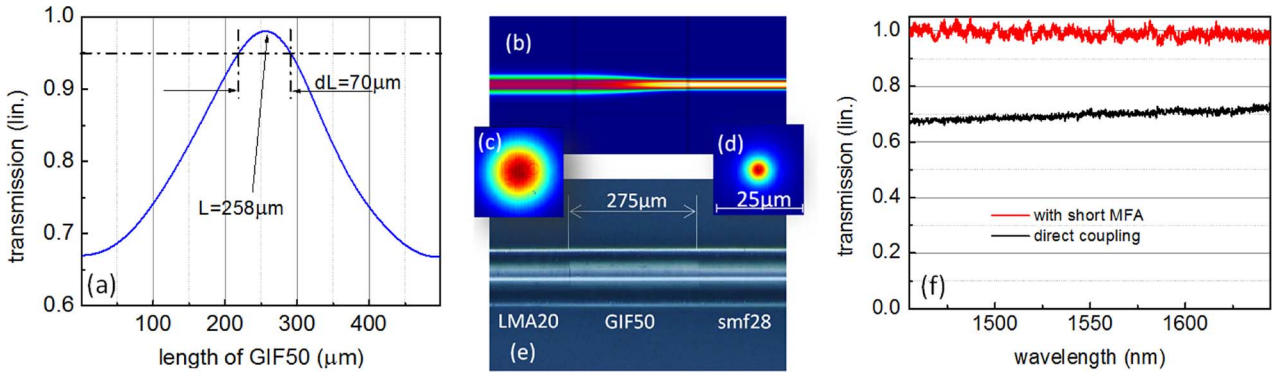

Fig. 13. Ultrashort MFA with less than 1 mm length, $> 95\%$ transmission and broad spectral transmission band. (a) Calculated transmission (1550 nm) scanning the length of a GIF50 segment between smf28e and LMA20. The first transmission maximum occurs for a GIF50 length of 258 μm. A length tolerance of several tens of microns is acceptable to achieve high transmission. (b) Calculated intensity distribution for light propagating through the MFA. (c) Near-field images of the in- and (d) output cross-sectional intensity distributions. (e) Microscope image of the actual device. (f) Transmission spectrum of the MFA device (blue line) compared to the transmission for directly spliced LMA 20-smf28e connection (black line).

fiber with a piece of GIF50 already spliced on was attached to a translation stage with 1 μm resolution. The subtle difference in refractive indexes between the two fibers makes it possible to see the splice. The fiber was then translated from the first splicing position by a distance of 258 μm. After cleaving and splicing to the output fiber, the MFA has been inspected once again under the microscope [see Fig. 13(e)]. Measurements of the length of the inserted GIF50 fiber revealed a length of 275 μm for the inserted GIMF, which is 17 μm longer than the targeted 258 μm. As shown in Fig. 13(a), this is close enough to obtain transmission values of about 95% both in simulation and experiment. As is expected, the results show a very low coupling loss [see Fig. 13(f)] that was constant over the whole measurement range from 1450 to 1650 nm. We believe that due to the simplicity and robustness of the design this type of MFA may have significant potential for large-scale production.

VI. Conclusion

In this paper, a detailed investigation of novel MFAs based on multimode interference in graded index fibers has been presented. We have shown that low-loss MFAs are indeed possible and can be designed to connect single-mode fibers with very different mode-fields. A large number of MFAs with different fibers have been fabricated and the transmission spectra have been analyzed. The spectra have been compared to a recently published analytical model [16] and excellent agreement has been found between predictions and experimental data. A method for wavelength tuning of the MFAs has been suggested and successfully tested. Finally, a very broadband MFA based on an extremely short multimode fiber segment has been demonstrated. The presented study will provide detailed guidelines for the design and fabrication of a novel type of low-loss single-mode fiber to single-mode fiber couplers that should prove very useful in a wide range of fiber-optic devices.

References

[1] A. Ishikura, Y. Kato, and M. Miyauchi, "Taper splice method for single-mode fibers," *Appl. Opt.*, vol. 25, no. 6, pp. 3460–3465, 1986.

[2] M. Kihara, S. Tomita, and M. Matsumoto, "Loss characteristics of thermally diffused expanded core fiber," *IEEE Photon. Technol. Lett.*, vol. 4, no. 12, pp. 1390–1391, Dec. 1992.

[3] K. Shigihara, K. Shiraishi, and S. Kawakami, "Modal field transforming fiber between dissimilar waveguides," *J. Appl. Phys.*, vol. 60, no. 4, pp. 4293–4296, 1986.

[4] M. Faucher and Y. K. Lize, "Mode field adaptation for high power fiber lasers," presented at the presented at the Conf. Lasers and Electro-Optics, San Jose, CA, 2007.

[5] S. W. Allison and G. T. Gillies, "Observations of and applications for self-imaging in optical fibers," *Appl. Opt.*, vol. 33, no. 4, pp. 1802–1805, 1994.

[6] L. B. Soldano and E. C. M. Pennings, "Optical multi-mode interference devices based on self-imaging: Principles and applications," *J. Lightw. Technol.*, vol. 13, no. 4, pp. 615–627, Apr. 1995.

[7] H. Li, M. Brio, L. Li, A. Schülzgen, N. Peyghambarian, and J. V. Moloney, "Multimode interference in circular step-index fibers studied with the mode expansion approach," *J. Opt. Soc. Am. B*, vol. 24, no. 14, pp. 2707–2720, 2007.

[8] X. Zhu, A. Schülzgen, H. Li, L. Li, L. Han, J. V. Moloney, and N. Peyghambarian, "Detailed investigation of self-imaging in largecore multimode optical fibers for application in fiber lasers and amplifiers," *Opt. Exp.*, vol. 16, pp. 16632–16645, 2008.

[9] W. S. Mohammed, A. Mehta, and E. G. Johnson, "Wavelength tunable fiber lens based on multimode interference," *J. Lightw. Technol.*, vol. 22, no. 2, pp. 469–477, Feb. 2004.

[10] Q. W. A. G. Farrell, "All-fiber multimode-interference-based refractometer sensor: Proposal and design," *Opt. Lett.*, vol. 31, pp. 317–319, 2006.

[11] W. S. Mohammed and P. W. E. Smith, "All-fiber multimode interference bandpass filter," *Opt. Lett.*, vol. 31, no. 3, pp. 2547–2549, 2006.

[12] X. Zhu, A. Schülzgen, H. Li, L. Li, Q. Wang, S. Suzuki, V. L. Temyanko, J. V. Moloney, and N. Peyghambarian, "Single-transverse-mode output from a fiber laser based on multimode interference," *Opt. Lett.*, vol. 33, pp. 908–910, 2008.

[13] A. C.-G. J. E. Antonio-Lopez, D. A. May-Arrioja, R. Selvas-Aguilar, and P. LiKamWa, "Tunable multimode-interference bandpass fiber filter," *Opt. Lett.*, vol. 35, pp. 324–326, 2010.

[14] X. Zhu, A. Schülzgen, H. Wei, K. Kieu, and N. Peyghambarian, "White light Bessel-like beams generated by miniature all-fiber device," *Opt. Exp.*, vol. 19, no. 10, pp. 11366–11375, 2011.

[15] A. H. Morshed, "Self-imaging in single mode-multimode-single mode optical fiber sensors," in *Proc. Saudi Int. Electron., Commun. Photonics Conf.*, Riyadh, Saudi Arabia, 2011, no. 5.

[16] A. Mafi, P. Hofmann, C. Jollivet-Salvin, and A. Schülzgen, "Low-loss coupling between two single-mode optical fibers with different mode-field diameters using a graded-index multimode optical fiber," *Opt. Lett.*, vol. 36, no. 3, pp. 3596–3598, 2011.

[17] K. Shiraishi, H. Ohnuki, N. Hiraguri, K. Matsumura, I. Ohishi, and H. Kazami, "A lensed-fiber coupling scheme utilizing a graded index fiber and a hemispherically ended coreless fiber tip," *J. Lightw. Technol.*, vol. 15, no. 8, pp. 356–363, Feb. 1997.

[18] Y. Mao, S. Chang, S. Sherif, and C. Flueraru, "Graded-index fiber lens proposed for ultrasmall probes used in biomedical imaging," *Appl. Opt.*, vol. 46, no. 8, pp. 5887–5894, 2007.
[19] Y. Mao, S. Chang, and C. Flueraru, "Fiber lenses for ultra-small probes used in optical coherent tomography," *J. Biomed. Sci. Eng.*, vol. 3, no. 8, pp. 27–34, 2010.
[20] I. H. Malitson, "Interspecimen comparison of the refractive index of fused silica," *J. Opt. Soc. Am.*, vol. 55, no. 5, pp. 1205–1209, 1965.
[21] D. Marcuse, "Loss analysis of single-mode fiber splices," *The Bell Syst. Tech. J.*, vol. 56, no. 16, pp. 703–718, 1977.
[22] W. T. Anderson, L. C. V. Shah, A. J. Johnson, and J. P. Kilmer, "Mode-field diameter measurements for single-mode fibers with non-gaussian field profiles," *J. Lightw. Technol.*, vol. LT-5, no. 2, pp. 211–217, Feb. 1987.
[23] M. Artiglia, G. Coppa, P. D. Vita, M. Potenza, and A. Sharma, "Mode field diameter measurements in single mode optical fibers," *J. Lightw. Technol.*, vol. 7, no. 8, pp. 1139–1152, Aug. 1989.

Author biographies not included at authors' request due to space constraints.